Islanded Microgrids Reconfiguration by Using Simple and Efficient Static Voltage Stability Index

Mohammad Hasan Hemmatpou[1,*], Mohsen Mohammadian[2], Ali-Akbar Gharaveisi[3]

Received: 2015 /05/23 Accepted: 2015 /08 /23

Abstract

Microgrids as the "building blocks of smart grids"are predicted to play a major role in the future, as they are capable of improving the technical, environmental and economic fields in large power systems. This paper proposes a new formulation for the islanded Microgrid reconfiguration in order to improve voltage stability index. The formulated problem is solved using harmony search algorithm. The increasing loadability index of microgrids in the islanding mode is more important than the index of the grid-connected mode due to its operational limitations such as reactive power generation. In addition, this paper presented an improved indicator to estimate the voltage stability margin of islanded microgrid system based on the system's operational constraints both saddle node and limited induced bifurcations, called as *cat_VSI*$_{IMG}$. The *cat_VSI*$_{IMG}$ which is validated by verified CPF method for IMGs is called the maximum load ability margin of IMG, λ_{IMG}. Performance and effectiveness of the proposed method are demonstrated on 33-bus test system. The results show that the implementation of appropriate IMG reconfiguration problem formulations will facilitate a successful integration of the microgrid concept in power systems.

Keywords: islanded microgrid; islanded microgrid reconfiguration; reduced islanded microgrid network; voltage stability; ZIP model.

Nomenclature

A. Parameters and Variables

r_{ij}	the *i-j* line resistance
x_{ij}	the *i-j* line reactance
L_{ij}	the *i-j* line inductance
w_i	Steady-state frequency of droop-controlled DG units
f	the operational frequency of IMG.
$\|V_i\|$	the voltage magnitude of bus *i*
$\|V_i\|^*, w_i^*$	No-load output voltage magnitude and frequency of droop-controlled DG unit at bus *i*, respectively
m, n	the sending and receiving bus
m_{pi} , n_{qi}	Active and reactive power static-droop gains for droop-controlled DG unit at bus *i*
$\lambda_{\max}$	the critical lading factor
P'_{Gi}	DG active power
Q'_{Gi}	DG reactive power
P_n (Q_n)	the active (reactive) loads at the bus n plus the active (reactive) power losses of the branch
$\tan(\varphi)$	load power factor
BIBC	bus current injections and the branch current
BCBV	branch currents and the bus voltage
ILF	IMG load flow
b	the number of branches
R_{mn} , X_{mn}	the resistance and reactance between bus m and n
R_l	the resistance of the line *l*
B_l	the current passing through line *l*
N	the number of RINs
λ_{RIN_i}	loading factor of *ith* RIN
k	step length control
λ	the loadability factor
P_{L0} ,Q_{L0}	the initial active and reactive power load, respectively
λ'	the power directions

B. Acronyms

CPF	continuation power flow
DG	distributed generation
MG	microgrid
IMG	islanded microgrid
IMGR	islanded microgrid reconfiguration
RIN	reduced IMG network
RN	reduced network
OPF	optimal power flow
PCC	point of common coupling

1. Introduction

The configuration and limitation of IMGs have resulted in voltage stability boundaries. If IMGs managed efficiently, distinct benefits can be provided. For this purpose, powerful toolboxes are developed to access the voltage stability index by considering IMG modelling and its operational limitations. These toolboxes can be

[1,*] PhD Student in Department of Electrical Engineering, Shahid Bahonar University of Kerman, Kerman, Iran, m.hematpour@eng.uk.ac.ir

[2] Assistant Professor in Department of Electrical Engineering, Shahid University of Kerman, Kerman, Iran, M.Mohammadian@uk.ac.ir

[3]Assistant Professor in Department of Electrical Engineering, Shahid University of Kerman, Kerman, Iran, a_gharaveisi@uk.ac.ir

used in IMGR, as specific tools, for efficient management of IMG operation and delay in renewing MG's infrastructures. In order to solve the proposed problem, an HSA is used for finding the best configuration of IMG for maximizing the voltage stability index.

A MG can be recognized as an integrated system, which is capable of operation in both grid-connected and islanded operation modes at the PCC [1]. This paper focuses exclusively on the islanded mode operation and therefore control strategies of DGs are discussed briefly in the following.

There are several strategies for control DGs in IMGs among these strategies the droop control has been widely used for sharing power between distributed generations [2], [3]. In this strategy, the power sharing is acquired by mimicking the behaviour of synchronous generators operating in parallel [4]. To do that, the frequency and the voltage of DG units are drooped by increasing of the active and reactive power, respectively [5]. In fact, this strategy is aimed to specify the static droop gains [6].

With the development of national economies and the improvement of people's lives, load demands are sharply increasing and the operating conditions of the active distribution systems are closer to the system boundaries. MG as a part of these systems does not exclude from this concept and is more tangible in IMG owing to absence of main grid and its operational limits, especially as the maximum generation capacity of DGs. MGs experience a distinct change from low to high load levels in islanding mode. Under certain critical loading conditions, IMGs may experience a voltage collapse. Hence, voltage stability is considered to be one of the keen interest of industry and research sectors around the world.

Over the last several years, a lot of attention has been devoted to MGs in technical, environmental and economic fields [7]. Although voltage stability is related to technical issue, but it might affect the economic aspect of MGs as well. Therefore, it is important to consider this issue in MG studies. Voltage stability is the ability of a system to maintain voltage, which is closely associated with power delivering capability of power system [8]. The voltage instability is not a new phenomenon for power system practicing engineers and researchers, but a few researchers have focused on the effect of these phenomena on the MGs especially the islanded ones. The decline of the voltage stability level is one of the important factors that restricts the increase of loads served by IMGs. Hence, it is necessary to consider voltage stability constraints on the planning and operation of IMGs. Some of the studies in this field are reviewed in continuing. In [9], the stability voltage stability of all buses in IMG considering different types of load models. In this case, the bus with the smallest value is more sensitive to voltage collapse. The proposed index is a powerful tool for conducting issue in MGs is divided into three categories, i.e. small signal, transient and voltage stability. In the mentioned paper, the small signal stability is analysed with a linearized model of micro sources and loads. In addition, the transient stability of a MG is assessed with a nonlinear model. This paper also describes that P-V and Q-V curves have useful information in the voltage stability study. The P-V curve indicates the maximum loadability while Q-V curve shows the necessary amount of reactive power at the load end for desired voltage. In order to analyze the dynamic voltage stability of MGs it is used to the dynamic model of autonomous MGs in [10]. The dynamic voltage stability index is evaluated by the conventional CPF. In [11], the maximum static loadability is considered in the operation of droop-controlled IMG. OPF solution has been used for calculating maximum loadability in this system. The final aim was to solve bi-objective OPF problem for loadability maximization and generation cost minimization as a techno-economic problem.

MGR like radial network reconfiguration is an instrument for configuration of MG to improve the technical operation of MGs under normal and abnormal conditions. Authors in [12] analyzes the network reconfiguration of MG by conventional manner on the basis of the mathematical model. MGR is established in order to improve the reliability parameters of the MGs. In [13], MGR is used to restore service to a section or to meet some operational requirements of dropping minimum loads of MG. It offers novel real-time implementation of intelligent algorithm for MGR. Shariatzadeh et al. used a genetic algorithm (GA) and graph theory for reconfiguration of 8-bus shipboard power system and modified CERTS microgrids with consideration of distributed generation and islanding operation mode [14]. In [15] Shao et al., presented a multi-agent system based approach for microgrid reconfiguration in order to minimize the loss of load under system and unit constraints. Ding et al., presented a hierarchical decentralized agent-based network reconfiguration methodology to minimize power losses for smart distribution systems [16], [17]. In these researches, a two-stage method is defined for coordinating the reconfigurations of decomposed subsystems.

As seen, the past researches contained useful methods for the distribution systems and grid connected microgrids reconfiguration. Therefore, it is necessary to pay attention to the islanded microgrid reconfiguration. Inspired by the past studies, we use a HSA for IMGR that maximize the voltage stability index. In this paper, an improved index is suggested for calculating the

operational studies such as MG and IMG reconfiguration by centralized and decentralized structure of MG. In fact, for better calculation of power flows in IMG, the grid is split into several RNs that the weakest RN is the one,

which includes the weakest bus. In this research, the 33-bus MG test systems are used to illustrate the performance of the proposed methodology.

The rest of this article is organized as follows. Section 2 describes IMG model. Section 3 explains problem formulation. Section 4 provides Generalization of the proposed voltage stability index for n-bus IMG. Section 5 demonstrates the numerical results of applying the proposed method to a test system. Finally, section 6 brings a conclusion obtained from an experiment reported in this article.

2. IMG model

MG as the building blocks of smart grids is a new network structure. Therefore, it is necessary to establish a new model considering the characteristics of the MG such as the operating modes of DGs in MGs. In grid-connected mode, the main grid specifies the frequency of the whole network. However, in the islanded mode, the frequency is determined through the sharing power between DGs by the droop control strategy.

By considering above notification, a brief view of IMG components is given in this section in order to present the problem formulation.

2.1. Branches

The branch is modelled as an impedance series $z_{ij} = r_{ij} + jx_{ij}$, in which $x_{ij} = w \times L_{ij} = 2 \times \pi \times f \times L_{ij}$.

2.2. Distributed Generators

In grid-connected mode, the upstream power network which supplies the MG and is substituted with an equivalent generator is treated as slack bus. Similar to traditional power flow studies, here DGs can be treated as PV and/or PQ buses. Adversely, in islanded mode, there is no slack bus anymore and DGs operation is governed by droop characteristics. This characteristic can be represented as [2]:

$$P_{Gi} = (\mathrm{w}_i^* - |w_i|) / \mathrm{m}_{p_i} \qquad (1)$$

$$Q_{Gi} = (\mathrm{V}_i^* - |V_i|) / \mathrm{n}_{p_i} \qquad (2)$$

The output impedance of the converter can be determined the droop characteristic. In the general case, it is assumed that both *R* and *X* are the resistance and reactance of converter, respectively. In [18], an orthogonal linear rotational transformation matrix T from active and reactive power *P* and *Q* to the "modified" active and reactive power P' and Q' is proposed as below:

$$\begin{bmatrix} P' \\ Q' \end{bmatrix} = T \begin{bmatrix} P \\ Q \end{bmatrix} = \begin{bmatrix} X/Z & -R/Z \\ R/Z & X/Z \end{bmatrix} \begin{bmatrix} P \\ Q \end{bmatrix} \qquad (3)$$

Droop-controlled DG is a control strategy in controllable DGs in IMGs that the droop curves of the droop-controlled inverter determine the frequency of IMG and the voltage magnitudes of the DGs. The droop-controlled characteristics determine how they perform in the IMG. The relation between P'_{Gi} and *w* can be given as [11]:

$$w = w_i^* - m_{pi} \times P'_{Gi} \qquad (4)$$

Similarly, the relation between $|V_i|$ and Q'_{Gi}, is described by below equation.

$$|V_i| = |V_i|^* - n_{qi} \times Q'_{Gi} \qquad (5)$$

The droop-controlled-DG is modelled as an ideal voltage source and its voltage magnitude and frequency are determined using the droop characteristic given in (4) and (5) [11].

As it can be seen from (3), for mainly inductive output impedance of converter $P'_{G_i} \cong P_{G_i}$, $Q'_{G_i} \cong Q_{G_i}$ whereas for mainly resistive one $P'_{G_i} \cong -Q_{G_i}$, $Q'_{G_i} \cong P_{G_i}$.

It can be easily concluded from the coupled inductor at the converter and the large inductor of the output filter or by using the virtual inductive output impedance that the output impedance of the converter is inductive [5]. This conclusion is compliance with IEEE 1547.7 for DG in IMG.

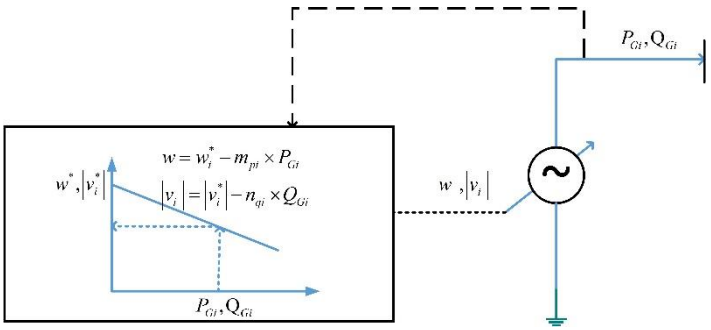

Figure 1. Steady-state model of DG unit in droop mode [11]

2.3. Loads

From a practical viewpoint, MG has different types of load such as residential, industrial and commercial loads. To quantify the influence of these variable loads on voltage stability, static load models as an algebraic function of the bus voltage magnitude and frequency at any instant time are used [8], [19]. The exponential active and reactive power load models are defined mathematically using equations (6) and (7):

$$P_i = P_0 \left(\frac{V_i}{V_0} \right)^{k_{pvi}} \left(\frac{f}{f_0} \right)^{k_{pfi}} \qquad (6)$$

$$Q_i = Q_0 \left(\frac{V_i}{V_0} \right)^{k_{qvi}} \left(\frac{f}{f_0} \right)^{k_{qfi}} \qquad (7)$$

3. Problem formulation

3.1. The objective function

The reconfiguration of IMG discussed in this paper is aimed at maximizing the system loadability limit. A HSA algorithm is used to find the optimal configuration of the switches in the network. At each iteration, the voltage stability index is evaluated by using development voltage stability index described in section 3.2. A brief discussion

regarding using the HSA algorithm in reconfiguration is presented in [20].

By increasing loads in the MGs, the concerns related to security challenges have been growing, increasingly. This subject is especially important in the island mode of MGs due to the absence of the main circuit and limitation of active and reactive power generation. There are two possible ways to improve the operation of IMGs. The first one is based on increasing investment for the better operation of IMGs, while the second one attempts to incorporate innovative solutions and technologies to change the technical specification of IMG. A significant amount of investment will be required to develop and to renew old infrastructures, while the most efficient way to meet social demands is to incorporate innovative solutions, technologies and grid architectures. Therefore, if IMGs managed efficiently, distinct benefits can be provided by IMGs. For this purpose, a powerful toolbox is developed to access the voltage stability index by considering IMG modelling and limits especially reactive generation limit. This toolbox can be used in operational studies of MGs and IMGs such as load shedding, reconfiguration and etc.

$$I_{mn} = \frac{|V_m| \prec \delta_m - |V_n| \prec \delta_n}{R_{mn} + jX_{mn}} \quad (8)$$

$$P_n - jQ_n = V_n^* I_{mn} \quad (9)$$

A new static bidirectional power flow algorithm is proposed to faithfully evaluate the voltage profile of IMG. A voltage stability index is presented for typical 2-bus system and then it will expand to a more sophisticated system including n-bus. So voltage stability index and power flow algorithm are briefly discussed.

Similar to the distribution systems, performance indices predict close to the voltage stability boundary are one of the great interest for researchers and technical staff in IMG operation. These performance indices are based on bifurcation points which refer to any fundamental change in system structural stability. It leads to instability of the system, and the saddle Node Bifurcation (SNB) and Limited Induced Bifurcation (LIB) are taken into account.

A SNB point, or point of collapse, is in coincidence with the singularity (zero eigenvalue) and the disappearance of the system steady-state load flow jacobian [21]. Encountering the operational limits or limitation of system equipment is the reason of a sudden system stability loss, known as LIB point. An LIB point is a sudden loss of system stability when a variable limit such as operational limits is encountered. This type of bifurcation can be the main reason of instability in IMGs due to their limitations. The SNB and LIB are explained briefly with regard to this division:

3.2.1 SNB

A static voltage stability index is derived from a relevant problem of power system analysis in IMGs. In this regard, an IMG is considered by two-bus test system

3.1. Voltage stability index

with neglecting the shunt capacitance that is valid for this system. It is assumed that this system is fed from a voltage stiff source without any limitation of active and reactive power generation. From Figure 2, the following equations can be written [22]:

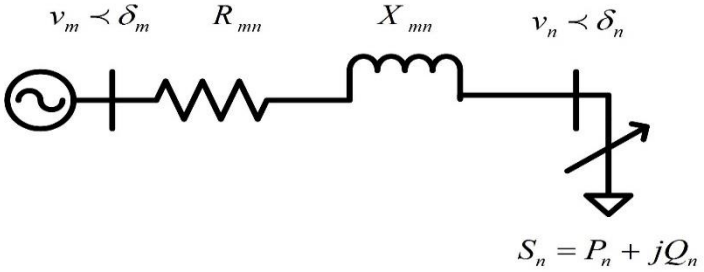

Figure 2. Two-bus equivalent model [22]

After some simple manipulations [23]:

$$|V_n|^4 + b_{mn}|V_n|^2 + h_{mn}|V_n| + c_{mn} = 0 \quad (10)$$

Where $b_{mn} = 2\left\{P_n R_{mn} + Q_n X_{mn} - \frac{|V_m|^2}{2}\right\}$, $h_{mn} = 0$ and $c_{mn} = Z_{mn}^2\left\{P_n^2 + Q_n^2\right\}$.

This equation represents the surface cusp catastrophe manifold in state space (V_n, b_{mn}, c_{mn}) and has four solutions which one of them is stable and can be written as below [23]:

$$V_n = \sqrt{\frac{-b_{mn} + \sqrt{d_{mn}}}{2}} \quad (11)$$

Where

$$d_{mn} = b_{mn}^2 - 4c_{mn} \quad (12)$$

The singularity point of equation (10) determines the SNB point and can be obtained through equating the derivative of equation (10) to zero [23].

$$2|V_n^{cr}|^3 + b_{mn}|V_n^{cr}| = 0 \Rightarrow |V_n^{cr}| = \sqrt{\frac{-b_{mn}}{2}} \quad (13)$$

Then, the critical lading factor $\lambda_{\max}$ is calculated by equation (14) [23]:

$$\lambda_{\max} = \frac{P_n^{\max}}{P_n^0} = \frac{1}{P_n^0} \times \left(\begin{array}{l} \frac{|V_m|^2}{2} \times \\ \left(|Z_{mn}| \sqrt{(1+\tan(\varphi)^2)} - \ldots \right. \\ \left. \frac{(R_{mn} + X_{mn}\tan(\varphi))}{(X_{mn} - R_{mn}\tan(\varphi))^2} \right) \end{array} \right) \quad (14)$$

As seen in equation (14) $\lambda_{\max}$ is a function of $Z_{mn} = R_{mn} + jX_{mn}$, $\tan(\varphi)$, $|V_m|$ and the base load at $\lambda = 1$ (P_n^0).

For the two-bus system shown in Figure2, authors in [23] introduced the voltage stability index of *n* named *VSI(n)* if d_{mn} in equation (12) is set to zero, then it can be defined as follows:

$$VSI(\mathrm{n}) = \left|V_m\right|^4 - 4\left[P_n X_{mn} - Q_n R_{mn}\right]^2 - ... \quad 4\left[P_n R_{mn} + Q_n X_{mn}\right]\left|V_m\right|^2 \tag{15}$$

cat_VSI determines the *SNB* of IMG and it is considered as voltage stability index of IMG. From the catastrophe theory point of view, the bifurcation set of an IMG which is given in equation (10) represents the boundary of the critical voltage region. The feasible and stable zone of the system is represented by the following equation [24]:

$$\left(\frac{b_{mn}}{2}\right)^2 - c_{mn} \geq 0 \tag{16}$$

cat_VSI(n) represents the voltage stability index based on catastrophe theory [24]:

$$cat\_VSI(\mathrm{n}) = \left(P_n R_{mn} + Q_n X_{mn} - 0.5\left|V_m\right|^2\right)^2 - ... \quad X_{mn}^2\left(P_m^2 + Q_m^2\right) \tag{17}$$

cat_VSI index can be variable from 0.25 (at no load) to 0 (at the collapse point). It is obvious that if the *cat_VSI* value is closer to 0.25, then the system is more stable.

Authors in [24] shows that the required time for calculation of *cat_VSI(n)* is less than the required time for *VSI* calculation; therefore, it can be used for online monitoring of the IMG state.

Unlike distribution system and grid-connected MG is sufficient to consider SNB [24], in IMG or stand-alone MG is also need to consider LIB due to the main rule of operational limitation especially reactive power generation.

Therefore, this paper develops a new and simple index for IMG named *cat_VSI*$_{IMG}$ to get a better and more useful voltage stability index through considering SNB and LIB.

3.2.2 LIB

As mentioned in section 2.2, the DG units, P_{Gi} and Q_{Gi} generation, are governed by the droop relations as mentioned in equations (4) and (5), up till their limitation, $P_{Gj}^{\max}$ and $Q_{Gj}^{\max}$, respectively, encounter. Beyond the $P_{Gj}^{\max}$ ($Q_{Gj}^{\max}$), the DG unit active (reactive) power generation does not follow the equations (4) and ((5)), and they have constant values of $P_{Gj}^{\max} = S_{Gj}^{\max}$ ($Q_{Gj}^{\max}$).

Therefore it is assumed that the two-bus system, is shown in Fig 2, is fed from a voltage source with limitation in active and reactive power generation.

Therefore, P_{Gj} at $Q_{Gj}^{\max}$ is obtained by equation (18):

$$P_{Gj}^{Q_{Gj}^{\max}} = \sqrt{\left(S_{Gj}^{\max}\right)^2 - \left(Q_{Gj}^{\max}\right)^2} \tag{18}$$

As mentioned before, LIBs defines voltage stability index due to operational limits such as generator reactive power limits and acceptable region frequency deviations [25], and the LIB point can be determined through solving the intersection of equations (9) and (19):

$$-P_m + jQ_m^{\max} = V_m^* I_{mn} \tag{19}$$

Based on equations (9) and (19), Q_n is obtained as function of $Q_m^{\max}$. This process is given in the following:

$$Q_m^{\max} - Q_n = X_{mn} I_{mn}^2 \tag{20}$$

By replacing I_{mn} from equation (19) in the equation (21), the mentioned relation is achieved.

$$S_m - S_n = Z_{mn}\left|I_{mn}\right|^2 \Rightarrow \quad (P_m - P_n) + j(Q_m^{\max} - Q_n) = ... \quad (R_{mn} + jX_{mn})\left|I_{mn}\right|^2 \tag{21}$$

$$Q_n = Q_m^{\max} - X_{mn}\left|\left(\frac{-P_m + jQ_m^{\max}}{V_m^*}\right)\right|^2 \tag{22}$$

$$P_n = P_m^{Q_m^{\max}} - R_{mn}\left|\left(\frac{-P_m + jQ_m^{\max}}{V_m^*}\right)\right|^2 \tag{23}$$

Therefore the state space (V_n, b_{mn}, c_{mn}) is affected by $Q_m^{\max}$. Then, the critical voltage at bus *n* is calculated by substituting equations (22) and (23) in equation (10). The receiving end voltage has only one physical solution that is positive and stable, named $\left|V_n^{cr}\right|$ at LIB. A simple 2-bus IMG system is used to provide an illustration of both SNB and LIB:

It can be seen that *cat_VSI* index can be varied from 0.25 (at no load) to the limited induced bifurcation (the collapse point) in the presence of operational limits. Otherwise it can be varied from 0.25 to 0 (at the collapse point).

4. Power flow algorithm and Generalization of the proposed index for n-bus IMG

This section presents a bidirectional electrical power flow algorithm in islanded MG. There is no slack bus and considered single-line balanced system. Therefore, the system frequency is one of the variables and it plays as a communication between the droop controlled DGs. The frequency of IMG has been determined by the sharing power between the droop-controlled DGs.

As explained in the section 2.2, a droop-controlled DG has been represented as an ideal voltage source with the active and reactive power injection described in (4) and (5). By exceeding the active and reactive power limitations in generating power with a droop-controlled DG, it switches from droop-mode to PQ mode and the specified power is kept at its limitation value [26]. The operation mode of each DGs, droop-controlled mode or PQ mode, in islanded MG plays an important role in the power flow algorithm. Therefore, the first step in the power flow is to identify the operation mode of each DG. The DGs must also supply the active (reactive) load and active (reactive) power losses.

Then, the next step is to define the direction of power flow by introducing a new concept named as RIN. The operation mode of each DGs and IMG structure identify RINs. A RIN is the only combination of the branches composing the trees connecting between two droop-controlled DG nodes or between a droop-controlled DG node and a downstream terminal node. This terminal node can contain a load bus or a DG-PQ bus.

For an effective explanation, a 10-bus IMG is suggested. This system is shown in Figure 3.a. It is assumed that three DG units exist are govern by droop control mode. By mentioning the DGs modes, this system is divided into two RINs, as shown in Figure 3.b and 3.c. To promote greater clarity, the RINs number 1 and 2 in Figure 3.b and Figure 3.c, are defined and explained. The RIN#1 is made up from the branch between the droop-controlled-DG number 1 and the terminal node (bus number 1). The power flow direction is from the bus number 2 to the bus number 1. The RIN#2 is made up from the branch between the droop-controlled DG#1 and the end terminal (bus#5), the droop-controlled DG#1 and between the droop-controlled DG#2.

As an example, the implementation details of ***ILF*** matrix of RIN#2 is explained in the following. It is assumed that DG#1 and DG#2 operate in the droop-controlled mode and V_2 and V_{10} are the magnitudes of the voltage at bus number 2 and 10, respectively. For determination of the power flow direction, it is firstly necessary to define a new concept named the deep point, if any exist. This basic concept is explained with examples in the following:

Two assumptions are essential to continue determination of deep point/points here. These are as follows:

1. DG#1 can supply the entire load bus number 2, 3, 4, 5, 6, 7 and the partial of load bus number 8 which is defined as μ, as shown in Figure 4.

2. DG #2 can supply load number 10, 9 and the partial load 8 defined as 1- μ.

The basic power flow analysis method used in this paper is graph theory like the method which used by Hemmatpour et al., [20]. As shown by them [20], ***BIBC*** matrix is the relationship between the bus current injections and the branch current. The ***BCBV*** matrix is the relationship between the branch currents and the bus voltage. By the combination of ***BIBC*** and ***BCBV***, the ***ILF*** matrix has been achieved. This matrix is the relationship between the bus current injection and the bus voltage; it is expressed by the following equation:

$$[\Delta \boldsymbol{V}] = [\boldsymbol{BCBV}][\boldsymbol{BIBC}][\boldsymbol{I}] = [\boldsymbol{ILF}][\boldsymbol{I}] \quad (24)$$

As a result, the deep point is the bus #8, and the ***BIBC***, ***BCBV*** and ***ILF*** can be obtained as follows:

$$[\boldsymbol{B}] = [\boldsymbol{BIBC}][\boldsymbol{I}] \Rightarrow$$

$$\begin{bmatrix} \boldsymbol{B}_1 \\ \boldsymbol{B}_2 \\ \boldsymbol{B}_3 \\ \boldsymbol{B}_4 \\ \boldsymbol{B}_5 \\ \boldsymbol{B}_6 \\ \boldsymbol{B}_7 \\ \boldsymbol{B}_8 \end{bmatrix} = \begin{bmatrix} 1 & 1 & 1 & 1 & 1 & 1 & 0 & 0 \\ 0 & 1 & 1 & 0 & 0 & 0 & 0 & 0 \\ 0 & 0 & 1 & 0 & 0 & 0 & 0 & 0 \\ 0 & 0 & 0 & 1 & 1 & 1 & 0 & 0 \\ 0 & 0 & 0 & 0 & 1 & 1 & 0 & 0 \\ 0 & 0 & 0 & 0 & 0 & 1 & 0 & 0 \\ 0 & 0 & 0 & 0 & 0 & 0 & 1 & 0 \\ 0 & 0 & 0 & 0 & 0 & 0 & 1 & 1 \end{bmatrix} \begin{bmatrix} \boldsymbol{I}_3 \\ \boldsymbol{I}_4 \\ \boldsymbol{I}_5 \\ \boldsymbol{I}_6 \\ \boldsymbol{I}_7 \\ \mu \boldsymbol{I}_8 \\ (1-\mu)\boldsymbol{I}_8 \\ \boldsymbol{I}_9 \end{bmatrix} \quad (25)$$

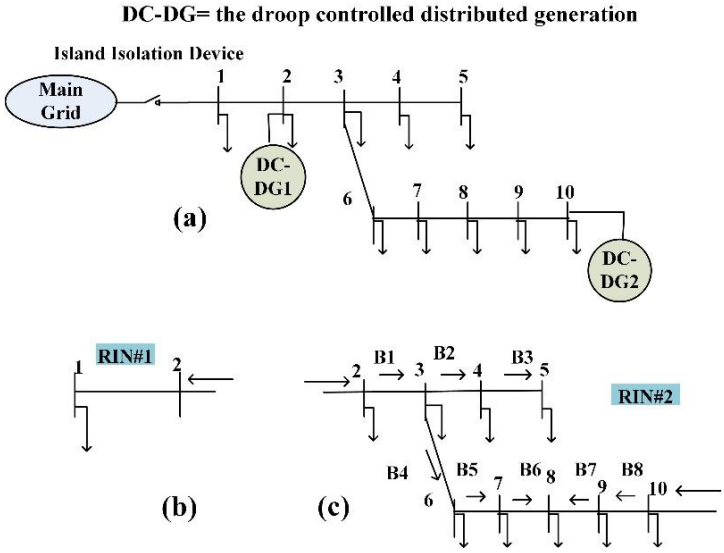

Figure 3. (a) 10-bus test system (b) RIN1 (c) RIN2

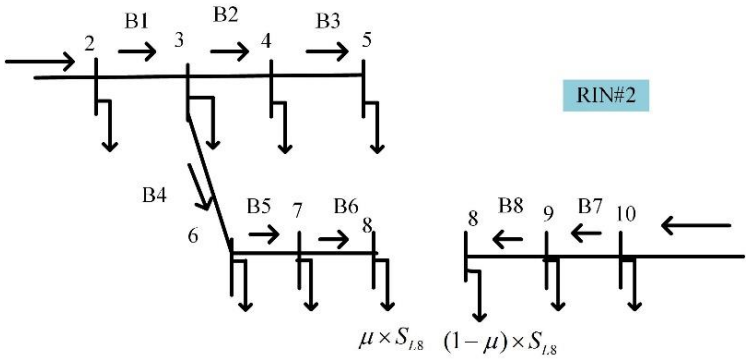

Figure 4. Illustration of deep point

By detection of the voltage magnitude and the voltage angle of each node, the active power losses is calculated as below:

$$P_{loss} = \sum_{l=1}^{b} R_l B_l^2 \quad (28)$$

$$[\Delta \boldsymbol{V}] = [\boldsymbol{BCBV}][\boldsymbol{B}] \Rightarrow \begin{bmatrix} \boldsymbol{V}_2 \\ \boldsymbol{V}_2 \\ \boldsymbol{V}_2 \\ \boldsymbol{V}_2 \\ \boldsymbol{V}_2 \\ \boldsymbol{V}_2 \\ \boldsymbol{V}_{10} \\ \boldsymbol{V}_{10} \end{bmatrix} - \begin{bmatrix} \boldsymbol{V}_3 \\ \boldsymbol{V}_4 \\ \boldsymbol{V}_5 \\ \boldsymbol{V}_6 \\ \boldsymbol{V}_7 \\ \boldsymbol{V}_8 \\ \boldsymbol{V}_9 \\ \boldsymbol{V}_8 \end{bmatrix} = \begin{bmatrix} \boldsymbol{Z}_{23} & 0 & 0 & 0 & 0 & 0 & 0 & 0 \\ \boldsymbol{Z}_{23} & \boldsymbol{Z}_{34} & 0 & 0 & 0 & 0 & 0 & 0 \\ \boldsymbol{Z}_{23} & \boldsymbol{Z}_{34} & \boldsymbol{Z}_{45} & 0 & 0 & 0 & 0 & 0 \\ \boldsymbol{Z}_{23} & 0 & 0 & \boldsymbol{Z}_{36} & 0 & 0 & 0 & 0 \\ \boldsymbol{Z}_{23} & 0 & 0 & \boldsymbol{Z}_{36} & \boldsymbol{Z}_{67} & 0 & 0 & 0 \\ \boldsymbol{Z}_{23} & 0 & 0 & \boldsymbol{Z}_{36} & \boldsymbol{Z}_{67} & \boldsymbol{Z}_{78} & 0 & 0 \\ 0 & 0 & 0 & 0 & 0 & 0 & 0 & \boldsymbol{Z}_{910} \\ 0 & 0 & 0 & 0 & 0 & 0 & \boldsymbol{Z}_{89} & \boldsymbol{Z}_{910} \end{bmatrix} \begin{bmatrix} \boldsymbol{B}_1 \\ \boldsymbol{B}_2 \\ \boldsymbol{B}_3 \\ \boldsymbol{B}_4 \\ \boldsymbol{B}_5 \\ \boldsymbol{B}_6 \\ \boldsymbol{B}_7 \\ \boldsymbol{B}_8 \end{bmatrix} \tag{26}$$

$$[\Delta \boldsymbol{V}] = [\boldsymbol{ILF}][\boldsymbol{I}] \Rightarrow \begin{bmatrix} \boldsymbol{V}_2 \\ \boldsymbol{V}_2 \\ \boldsymbol{V}_2 \\ \boldsymbol{V}_2 \\ \boldsymbol{V}_2 \\ \boldsymbol{V}_2 \\ \boldsymbol{V}_{10} \\ \boldsymbol{V}_{10} \end{bmatrix} - \begin{bmatrix} \boldsymbol{V}_3 \\ \boldsymbol{V}_4 \\ \boldsymbol{V}_5 \\ \boldsymbol{V}_6 \\ \boldsymbol{V}_7 \\ \boldsymbol{V}_8 \\ \boldsymbol{V}_9 \\ \boldsymbol{V}_8 \end{bmatrix} = \begin{bmatrix} \boldsymbol{Z}_{23} & 0 & 0 & 0 & 0 & 0 & 0 & 0 \\ \boldsymbol{Z}_{23} & \boldsymbol{Z}_{34} & 0 & 0 & 0 & 0 & 0 & 0 \\ \boldsymbol{Z}_{23} & \boldsymbol{Z}_{34} & \boldsymbol{Z}_{45} & 0 & 0 & 0 & 0 & 0 \\ \boldsymbol{Z}_{23} & 0 & 0 & \boldsymbol{Z}_{36} & 0 & 0 & 0 & 0 \\ \boldsymbol{Z}_{23} & 0 & 0 & \boldsymbol{Z}_{36} & \boldsymbol{Z}_{67} & 0 & 0 & 0 \\ \boldsymbol{Z}_{23} & 0 & 0 & \boldsymbol{Z}_{36} & \boldsymbol{Z}_{67} & \boldsymbol{Z}_{78} & 0 & 0 \\ 0 & 0 & 0 & 0 & 0 & 0 & 0 & \boldsymbol{Z}_{910} \\ 0 & 0 & 0 & 0 & 0 & 0 & \boldsymbol{Z}_{89} & \boldsymbol{Z}_{910} \end{bmatrix} \begin{bmatrix} 1 & 1 & 1 & 1 & 1 & 1 & 0 & 0 \\ 0 & 1 & 1 & 0 & 0 & 0 & 0 & 0 \\ 0 & 0 & 1 & 0 & 0 & 0 & 0 & 0 \\ 0 & 0 & 0 & 1 & 1 & 1 & 0 & 0 \\ 0 & 0 & 0 & 0 & 1 & 1 & 0 & 0 \\ 0 & 0 & 0 & 0 & 0 & 1 & 0 & 0 \\ 0 & 0 & 0 & 0 & 0 & 0 & 1 & 0 \\ 0 & 0 & 0 & 0 & 0 & 0 & 1 & 1 \end{bmatrix} \begin{bmatrix} \boldsymbol{I}_3 \\ \boldsymbol{I}_4 \\ \boldsymbol{I}_5 \\ \boldsymbol{I}_6 \\ \boldsymbol{I}_7 \\ \mu \boldsymbol{I}_8 \\ (1-\mu)\boldsymbol{I}_8 \\ \boldsymbol{I}_9 \end{bmatrix} \tag{27}$$

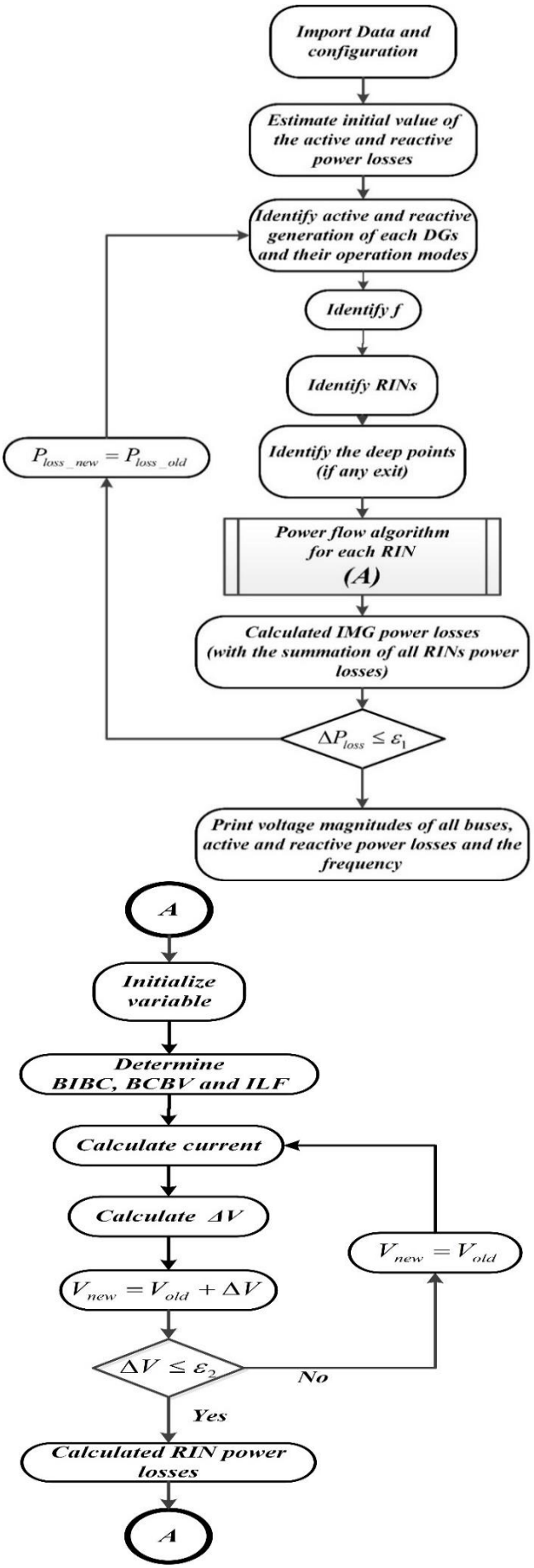

Figure 5. Power losses calculation flowchart

To gain power flow convergence, the algorithm is repeated until the accuracy of calculating the power losses reaches to a threshold defined by the user. The power flow algorithm is illustrated in Figure 5.

After determination of the RINs and power flow convergence, the proposed index is generalized to n-bus IMG. The method used to generalize *cat_VSI* depends on the RINs and deep point/points to the reduction of IMG into an equivalent two-bus system, which compute the parameters of the equations (15) and (17) as follows:

P_n and Q_n are the sum of the active and reactive loads of all the buses beyond bus *n*, the active and reactive power load of bus *n* itself, and the sum of the active and reactive power losses of all the branches beyond node *n*.

Since an IMG may consist of more than one *RIN*, the cat_VSI_{IMG} is calculated through equation (29).

$$cat\_VSI_{IMG} = \min\begin{Bmatrix} cat\_VSI_{RIN_1}, cat\_VSI_{RIN_2}, \\ ..., cat\_VSI_{RIN_N} \end{Bmatrix} \quad (29)$$

N, is the number of *RINs*, existed in the islanded microgrid. The $cat\_VSI_{RIN_i}$ is used to detect the voltage stability of the *ith* RIN. The region with minimum cat_VSI_{RIN} defined the critical *RIN* and the bus with minimum stability index in this *RIN* is the most sensitive bus to the voltage collapse and it has been known as the critical bus.

5. Results and discussion

In this research, 33-bus IMG is used in order to demonstrate the effectiveness of the proposed method. The simulation has been carried out using MATLAB software, in the Centre for Renewable Energy Research of Shahid Bahonar university of Kerman, Kerman, Iran.
The location and technical information of DGs including DGs locations, static droop coefficients, nominal setting and ratings are shown in Table 1. The load data and the feeder data of the test system are given in [27].

Table 1. The location and technical information of DGs in the 33- bus IMG [27]

DG No.	Location	m_p p.u.	n_q p.u.	w^* p.u.	v^* p.u.	S^{max} p.u	Q^{max} p.u.
1	4	1.126e-3	1/40	1	1.01	2	1.2
2	8	1.501e-3	1/30	1	1.01	1.5	0.9
3	22	4.504e-3	1/10	1	1.01	0.5	0.3
4	25	1.126e-3	1/40	1	1.01	2	1.2
5	33	2.252e-3	1/20	1	1.01	1	0.6

5.1. The base configuration

The base IMG configuration and its' RINs are shown in Figure 6, the results for this system at different load types are given in Table 2. From this table it is readily seen that the RIN2 is the weakest and the bus 29 due to its minimized value of stability index is the most disposed bus to instability. To validate the proposed method, the obtained results from the *cat_VSI* are compared with the proposed CPF for IMG to ascertain its effectiveness.

More details of this proposed CPF method are given in section 7 (Appendix). The loadability index (λ) is

obtained by gradual increase in steps until to reach the LIB or SNB limits. The increasing load factor (λ_{IMG}) is obtained 1.765 and 1.769 by the proposed CPF method and *cat_VSI* for constant power, respectively. The difference between the two results is 0.2266%; in other words, the proposed CPF method confirms the proposed *cat_VSI* index. Comparison of the two proposed method shows that for IMG, the proposed *cat_VSI* index compared to the proposed CPF is faster and it is an authoritative method for the large scale MG in the islanded- or grid-connected modes. The CPF method does not converge for large scale MG due to singularity of its sparse matrixes.

The allowable change limit of the IMGs frequency deviation is ±0.1 Hz in Nordel (North of Europe) and ±0.2Hz in UCTE (Union for the Co-ordination of Transmission of Electricity, Continental Europe) [4]. In this paper, the ±0.1 Hz and ±0.2Hz frequency deviation are considered as a strict and frequent acceptable regions that are defined by the operating point with frequency bigger than 0.9983 (p.u.) and 0.9967(p.u.), respectively. Figure 7 shows the system frequency as a function of the increasing load factor. It can be seen that the system frequency is in the allowable deviation tolerance as the system loading increase. If the ±0.1 Hz frequency deviation has been considered as the LIB, the system loadability is enforced in $\lambda = 1.395$.

For instance, Table 3 shows the active, reactive and apparent power production by the different DGs in $\lambda = 1$ and $\lambda = 1.769$ at constant load impedance model. It can be seen that with the increase of the system loading, the active and reactive power generation is correctly governed by the droop controlled DG units (4) and (5) and when each of them reach to their maximum capability such as DG unit #3, they are being governed by their complementary constraints ($P_{Gj}^{\max}$ and $Q_{Gj}^{\max}$).

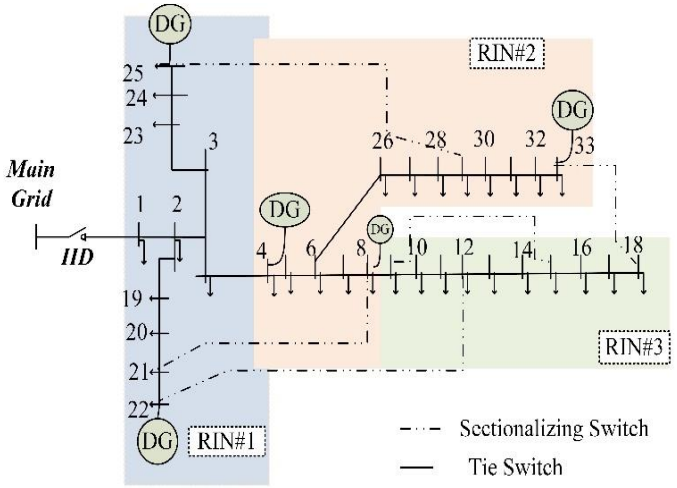

Figure 6. RIN regions of the base configuration

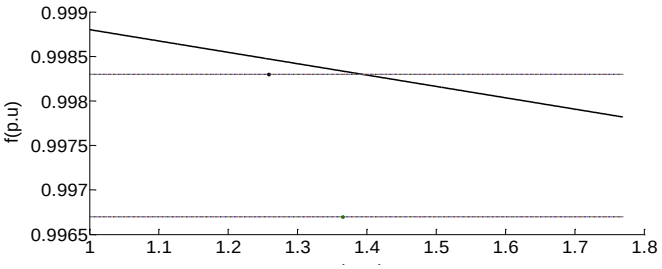

Figure 7. System frequency as a function of λ

Table 2. Bus voltages and stability index at different load types for 33-bus IMG

Bus No.	Load Flow Bus Voltage			VSI			IMG_index					
							Const. power		Const. current		Const. imped.	
	Const. power	Const. current	Const. imped.	Const. power	Const. current	Const. imped.	cat_VSI	V_{cr}	cat_VSI	V_{cr}	cat_VSI	V_{cr}
1	0.992830588	0.99284126	0.992852	0.989327	0.989321	0.989315	0.239496	0.989327	0.23949	0.989321	0.239485	0.989315
2	0.992830588	0.99284126	0.992852	0.957985	0.957962	0.957938	0.239496	0.989327	0.23949	0.989321	0.239485	0.989315
3	0.977090667	0.97720832	0.977324	0.846368	0.847482	0.848559	0.211592	0.959157	0.21187	0.959473	0.21214	0.959778
4	0.994384939	0.99438501	0.994385	0.963542	0.963484	0.963426	0.240885	0.992271	0.240871	0.992246	0.240856	0.99222
5	0.991834596	0.99184534	0.991856	0.94318	0.943222	0.943263	0.235795	0.985482	0.235806	0.985493	0.235816	0.985504
6	0.976472946	0.97650873	0.976544	0.950615	0.950658	0.9507	0.237654	0.987418	0.237664	0.987429	0.237675	0.98744
7	0.976623815	0.9766561	0.976688	0.951632	0.951664	0.951695	0.237908	0.987682	0.237916	0.987691	0.237924	0.987699
8	0.95804011	0.95812296	0.958198	0.885077	0.885884	0.88667	0.221269	0.980748	0.221471	0.980748	0.221667	0.980746
9	0.951885407	0.95223936	0.952573	0.885077	0.885884	0.886669	0.221269	0.969941	0.221471	0.970162	0.221667	0.970377
10	0.946176777	0.94678245	0.947355	0.849022	0.850534	0.852012	0.212255	0.959908	0.212633	0.960335	0.213003	0.960752
11	0.945332504	0.94597542	0.946584	0.843784	0.845397	0.846973	0.210946	0.958424	0.211349	0.958882	0.211743	0.959329
12	0.943860405	0.94456831	0.945238	0.834702	0.836488	0.838235	0.208676	0.955835	0.209122	0.956346	0.209559	0.956845
13	0.937859862	0.93883325	0.939756	0.79838	0.800847	0.803263	0.199595	0.945263	0.200212	0.945992	0.200816	0.946705
14	0.935634921	0.93670685	0.937723	0.785208	0.787917	0.79057	0.196302	0.941339	0.196979	0.94215	0.197643	0.942942
15	0.934248711	0.93538208	0.936457	0.777079	0.779935	0.782733	0.19427	0.938894	0.194984	0.939755	0.195683	0.940597
16	0.932906094	0.934099	0.93523	0.769263	0.772259	0.775196	0.192316	0.936524	0.193065	0.937434	0.193799	0.938324
17	0.930916442	0.93219766	0.933413	0.757782	0.760983	0.764121	0.189446	0.93301	0.190246	0.933993	0.19103	0.934955
18	0.930320619	0.93162827	0.932869	0.75437	0.75763	0.760828	0.188592	0.931958	0.189408	0.932963	0.190207	0.933946
19	0.988142156	0.98817822	0.988214	0.957095	0.957074	0.957054	0.239274	0.989097	0.239269	0.989091	0.239264	0.989086
20	0.989339353	0.98936432	0.989389	0.957096	0.957035	0.956974	0.239274	0.989097	0.239259	0.989081	0.239244	0.989066
21	0.990046117	0.99006454	0.990083	0.959751	0.959656	0.959561	0.239938	0.989782	0.239914	0.989758	0.23989	0.989733
22	0.991963788	0.99196446	0.991965	0.969189	0.968992	0.968797	0.242297	0.992207	0.242248	0.992156	0.242199	0.992106
23	0.97742872	0.97754039	0.97765	0.84852	0.849571	0.850588	0.21213	0.959767	0.212393	0.960064	0.212647	0.960351
24	0.978868197	0.97895438	0.979039	0.85773	0.858513	0.859268	0.214432	0.96236	0.214628	0.96258	0.214817	0.962791
25	0.983593754	0.98359637	0.983599	0.85773	0.858513	0.859268	0.214433	0.970868	0.214628	0.970833	0.214817	0.970797
26	0.988779318	0.98881501	0.98885	0.922447	0.922754	0.923057	0.230612	0.980021	0.230689	0.980103	0.230764	0.980183
27	0.988242654	0.98828273	0.988322	0.91884	0.919192	0.91954	0.22971	0.979061	0.229798	0.979155	0.229885	0.979248
28	0.986502009	0.98655632	0.98661	0.907204	0.907703	0.908196	0.226801	0.975947	0.226926	0.976081	0.227049	0.976214
29	0.963555033	0.96389933	0.964235	0.639425	0.646003	0.651963	0.159856	0.894226	0.161501	0.896517	0.162991	0.898578
30	0.964066546	0.96439847	0.964722	0.642218	0.648586	0.654351	0.160555	0.895201	0.162147	0.897412	0.163588	0.8994
31	0.970263369	0.97044534	0.970622	0.67679	0.680498	0.683803	0.169198	0.907013	0.170125	0.908253	0.170951	0.909354
32	0.972939701	0.97305698	0.973171	0.692129	0.694626	0.696817	0.173032	0.912109	0.173657	0.912931	0.174204	0.91365
33	0.977315162	0.97732685	0.977338	0.692129	0.694626	0.696817	0.173032	0.920425	0.173657	0.920567	0.174204	0.920664

Table 3. DG Units' generation in $\lambda = 1$ and $\lambda = 1.769$ at constant load impedance

DG No.	$\lambda = 1$			$\lambda = 1.769$		
	P_G p.u.	Q_G p.u.	S_G p.u.	P_G p.u.	Q_G p.u.	S_G p.u.
1	1.069	0.658	1.255	1.925	1.174	2.255
2	0.802	0.503	0.947	1.444	0.898	1.700
3	0.267	0.167	0.315	0.4	0.3	0.5
4	1.069	0.658	1.255	1.925	1.174	2.255
5	0.534	0.335	0.630	0.962	0.599	1.133

5.2. Islanded Microgrid Reconfiguration

For this study, HSA is used to find the best configuration of this IMG [26]. The HMS is selected to be 20. The HMCR and evaluation number are set to 0.9 and 100, respectively. The PAR increases linearly from 0.44 and 0.99, in the HAS. Each harmony in the population is evaluated using equation (30), searching for the harmony associated with minimum fitness.

$$Min\ \mathrm{F} = \left(cat\_VSI_{IMG}^{base} - cat\_VSI_{IMG} \right) \qquad (30)$$

The securest case has the maximum loadability index is shown in Figure 8. The technical operating specifications of this point are summarized below:

The opening switches are: 10, 13, 19, 23 and 30.

The operating frequency at base case is: 0.998801 p.u. (in strict region).

The critical bus is: 30

The min(Cat_VSI) is: 0.2169

The increasing load factor is: 1.792.

The frequency at the maximum loadability point is: 0.997822 p.u. (in acceptable region).

It can be seen that the system frequency is in the allowable deviation tolerance as the system loading increase. If the ±0.1 Hz frequency deviation has been considered as the LIB, the system loadability is enforced in $\lambda = 1.405$.

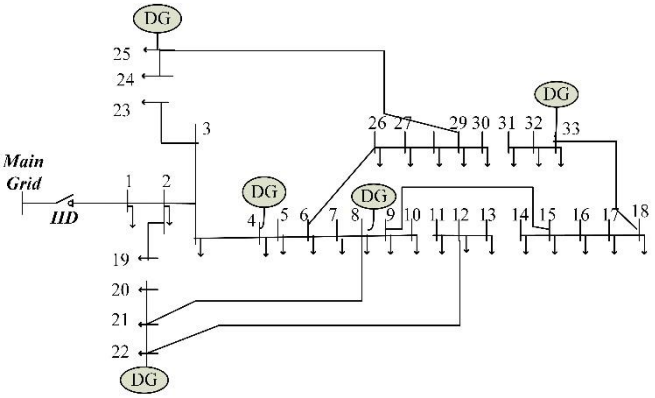

Figure 8. The securest configuration

6. Conclusion

This paper had presented a simple and efficient method for voltage stability assessment of islanded microgrids. Also it is used reconfiguration for

improvement voltage stability index in these systems. This powerful and generalized voltage stability index, called cat_VSI. In IMGs due to the absence of the main grid, there is no slack bus, so the frequency is obtained from the sharing power between DGs. In order to provide proper modelling of the IMG, the impact of frequency on all parts of the system such as feeders, loads and branches should be considered for generalization of this index. In the voltage stability calculation process, another efficient and useful index is introduced called RIN which is identified through the DGs operation mode and IMG configuration. The cat_VSI was verified using a proposed CPF method and successfully applied to 33-bus IMG for different load type conditions. Reconfiguration is used as an optimization tool for improvement voltage stability index. IMGR successfully applied to 33-bus IMG. Results show that the proposed index is robust and can provide useful information for the most sensitive bus to the voltage collapse at any operating point of IMGs. Finally, the results show that the proposed algorithm is a powerful and helpful tool for applications in the future control centre of IMG.

7. Appendix: Voltage stability index

Similar to the conventional power system [28], λ is considered as a voltage stability index in an IMG. λ_{IMG} is defined as a static voltage stability index to represent the closeness of the operating point and the voltage collapse point, as shown in Figure A1.

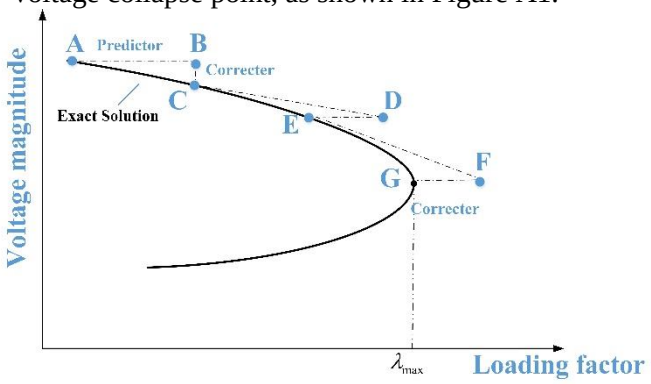

Figure A1 Continuation power flow theorem [28]

This paper provides a new and simple index as the λ_{IMG} to get a better estimation of the distance to voltage collapse. Practically, the IMG may consist of more than one *RINs*. The static voltage stability is designated by evaluating the λ of each RINs through (A.1). From (A.1), the weakest *RIN* is the one with the lowest value of lamda and it is prone to the voltage collapse.

$$\lambda_{IMG} = \min\left\{\lambda_{RIN_1}, \lambda_{RIN_2}, ..., \lambda_{RIN_N}\right\} \quad \text{(A.1)}$$

One of the proposed methods for calculation of λ_{IMG} is defined as Continuation power flow (CPF) based on bifurcation point/points. Since the *LIB* and *SNB* were briefly described in section 3.1, the CPF method is presented in the following:

7.1. CPF method

CPF is also called predictor-corrector methods since they involve the prediction of the next solution point and correction of the prediction to get the next point by tracing a curve with an initial point, as shown in FigureA1. The continuous process, as shown in FigureA1, can be diagrammatically shown as follows:

$$(x^j,\lambda^j) \xrightarrow{\text{Predictor}} (\hat{x}^{j+1},\hat{\lambda}^{j+1}) \xrightarrow{\text{Corrector}} (x^{j+1},\lambda^{j+1})$$

Where, (x^j,λ^j) represents the current solution, $(\hat{x}^{j+1},\hat{\lambda}^{j+1})$ is the predicted solution based on the computation of tangent vector, and (x^{j+1},λ^{j+1}) is the next solution on the curve.

The predictor step is based on the computation of the tangent vector and the corrector step is obtained either by means of a local parameterization or a perpendicular intersection [29]. λ is used to modify the connected load as shown below [29]:

$$\begin{cases} P_L = (1+\lambda')P_{L0} = \lambda P_{L0} \\ Q_L = (1+\lambda')Q_{L0} = \lambda Q_{L0} \end{cases} \quad \text{(A.2)}$$

To find out the process of the algorithm, consider a system of n nonlinear equation $g(x,\lambda)=0, x\in R$. The Predictor step is a procedure to find the next solution and the tangent vector ($z_j=[dx_j\ d\lambda_j]^T$) is used for estimating the next solution by the linearization method at the current equilibrium point (x^j,λ^j).

$$g\ (x_j,\lambda_j)\ =\ 0 \quad \text{(A.3)}$$

$$\frac{dg}{dx}|_{(x_j,\lambda_j)} = \nabla_x g\,|_{(x_j,\lambda_j)}\ \frac{dx}{d\lambda}|_{(x_j,\lambda_j)} + \frac{dg}{d\lambda}|_{(x_j,\lambda_j)} = 0 \quad \text{(A.4)}$$

The tangent vector can be approximated by following equation:

$$\tau\,|_{(x^j,\lambda^j)} = \frac{dx}{d\lambda}|_{(x_j,\lambda_j)} \approx \frac{\Delta x\,|_{(x_j,\lambda_j)}}{\Delta\lambda\,|_{(x_j,\lambda_j)}} \quad \text{(A.5)}$$

From the equations (A.4) and (A.5):

$$\tau\,|_{(x_j,\lambda_j)} = -\nabla_y g\,|^{-1}_{(x_j,\lambda_j)} \times \frac{dx}{d\lambda}|_{(x_j,\lambda_j)} \quad \text{(A.6)}$$

$$\Delta x\,|_{(x_j,\lambda_j)} = \tau\,|_{(x_j,\lambda_j)}\ \Delta\lambda\,|_{(x_j,\lambda_j)} \quad \text{(A.7)}$$

A step length control (k) is used for robustness of predictor algorithm. using k, the true direction and solution of predicted point is determined. The influence of this parameter is shown in the below equations [29]:

$$\Delta\lambda_{(x_j,\lambda_j)} \cong \frac{k}{\left\|\tau_{(x_j,\lambda_j)}\right\|} \quad \text{(A.8)}$$

$$\Delta y_{(x_j,\lambda_j)} \cong \frac{k\tau_{(x_j,\lambda_j)}}{\left\|\tau_{(x_j,\lambda_j)}\right\|} \quad \text{(A.9)}$$

The corrector step finds the next solution (x^{j+1},λ^{j+1}) using a topographic approach [30]. By adding an equation to $g(x,\lambda)=0$, x can be predicted with varying λ

, as showing in (A.10). The additional equation is a parameterized equation which identifies the location of the current solution with respect to the previous or next solution [22].

$$\begin{cases} g(\mathrm{x},\lambda)=0 \\ \rho(\mathrm{x},\lambda)=0 \end{cases} \qquad \text{(A.10)}$$

In this paper, the natural parameterization scheme has been used to quantify this relation which simply uses λ directly as the parameter, so the new λ is simply the previous value plus the step size, as shown in (A.11) [28].

$$\begin{cases} \rho(\mathrm{x},\lambda)=x_{ci}-(x_p+\Delta x_{pi}) \\ \textit{or} \\ \rho(\mathrm{x},\lambda)=\lambda_c-(\lambda_p+\Delta\lambda_p) \end{cases} \qquad \text{(A.11)}$$

8. Reference

[1] F. Katiraei and M. Iravani, "Power management strategies for a microgrid with multiple distributed generation units" Power Systems, IEEE Transactions on, 21, 2006, 1821-1831.

[2] P. Sreekumar, V. Khadkikar, "A New Virtual Harmonic Impedance Scheme for Harmonic Power Sharing in an Islanded Microgrid" Power Delivery, IEEE Transactions on, 2015, 1-10.

[3] M. Mehrasa, E.s Pouresmaeil, B. Nørregaard Jørgensen, and J. P.S. Catalão, "A control plan for the stable operation of microgrids during grid-connected and islanded modes" Electric Power Systems Research, 129, 2015, 10-22.

[4] J. M. Guerrero, J. C. Vasquez, J. Matas, L. G. de Vicuña, and M. Castilla, "Hierarchical control of droop-controlled AC and DC microgrids—a general approach toward standardization" Industrial Electronics, IEEE Transactions on, 58, 2011, 158-172.

[5] J. M. Guerrero, P. C. Loh, M. Chandorkar, and T.-L. Lee, "Advanced Control Architectures for Intelligent MicroGrids, Part I: Decentralized and Hierarchical ControlAdvanced Control Architectures for Intelligent Microgrids" IEEE Transactions on Industrial Electronics, 60, 2013, 1254-1262.

[6] Y. Liu, Q. Zhang, C. Wang, and N. Wang, "A control strategy for microgrid inverters based on adaptive three-order sliding mode and optimized droop controls" Electric Power Systems Research, 117, 2014, 192-201.

[7] N. Hatziargyriou, Microgrids: Architectures and Control, Wiley-IEEE Press, 2014, 10-12.

[8] P. Kundur, N. J. Balu, and M. G. Lauby, Power system stability and control, McGraw-hill New York, 1994.

[9] R. Majumder, "Some aspects of stability in microgrids" IEEE Transactions on power systems, 28, 2013, 3243-3252.

[10] G. Díaz, "Maximum loadability of droop regulated microgrids-formulation and analysis" Generation, Transmission & Distribution, IET, 7, 2013,

[11] M. Abdelaziz and E. El-Saadany, "Maximum loadability consideration in droop-controlled islanded microgrids optimal power flow" Electric Power Systems Research, 106, 2014, 168-179.

[12] X. Zhan, T. Xiang, H. Chen, B. Zhou, and Z. Yang, "Vulnerability assessment and reconfiguration of microgrid through search vector artificial physics optimization algorithm" International Journal of Electrical Power & Energy Systems, 62, 2014, 679-88.

[13] F. Shariatzadeh, CB. Vellaithurai, SS. Biswas, R. Zamora, and AK. Srivastava, "Real-Time Implementation of Intelligent Reconfiguration Algorithm for Microgrid" Sustainable Energy, IEEE Transactions on, 5, 2014, 598 - 607.

[14] F. Shariatzadeh, R. Zamora, and AK.Srivastava "Real time implementation of microgrid reconfiguration North" American Power Symposium (NAPS), 2011: IEEE, 2011, 1-6.

[15] C. Shao, C. Xu , S. He, X. Lin, and X. Li, "Operation of Microgrid Reconfiguration based on MAS (Multi-Agent System)" TENCON 2013-2013 IEEE Region 10 Conference (31194): IEEE, 2013, 1-4.

[16] D. Fei, and KA. Loparo, "Hierarchical Decentralized Network Reconfiguration for Smart Distribution Systems—Part I: Problem Formulation and Algorithm Development. Power Systems" IEEE Transactions on, 30, 2015, 734-43.

[17] D. Fei, and KA. Loparo, "Hierarchical Decentralized Network Reconfiguration for Smart Distribution Systems—Part II: Problem Formulation and Algorithm Development. Power Systems" IEEE Transactions on, 30, 2015, 744-52.

[18] K. De Brabandere,B. Bolsens, J. Van den Keybus, A. Woyte, J. Driesen, R. Belmans, "A Voltage and Frequency Droop Control Method for Parallel Inverters" Power Electronics, IEEE Transactions on, 22, 2007, 1107-15.

[19] A. El-Fergany, "Backtracking search algorithm to assign distributed generators in radial distribution systems comprising various load models" Applied Soft Computing, 30, 803-811.

[20] M. H. Hemmatpour, M. Mohammadian, and M. R. Estabragh, "A novel approach for the reconfiguration of distribution systems considering the voltage stability margin" Turkish Journal of Electrical Engineering & Computer Sciences, 21, 2013, 679-698.

[21] I. Dobson and L. Lu, "New methods for computing a closest saddle node bifurcation and worst case load power margin for voltage collapse" Power Systems, IEEE Transactions on, 8, 1993, 905-913.

[22] M. Chakravorty and D. Das, "Voltage stability analysis of radial distribution networks" International Journal of Electrical Power & Energy Systems, 23, 2001, 129-135.

[23] S. Chanda and B. Das, "Identification of weak buses in a power network using novel voltage stability indicator in radial distribution system" in Power Electronics (IICPE), 2010 India International Conference on, 2011, 1-4.

[24] G. A. Mahmoud, "Voltage stability analysis of radial distribution networks using catastrophe theory" Generation, Transmission & Distribution, IET, 6, 2012, 612-618.
[25] M. Federico, Power System Modelling and Scripting, Springer Berlin Heidelberg, 2010, 111-113.
[26] M. M. A. Abdelaziz, New Analysis and Operational Control Algorithms for Islanded Microgrid Systems, PhD thesis, University of Waterloo, 2014.
[27] M. R. Andervazh, J. Olamaei, and M. R. Haghifam, "Adaptive multi-objective distribution network reconfiguration using multi-objective discrete particles swarm optimisation algorithm and graph theory" Generation, Transmission & Distribution, IET, 7, 2013, 1367-1382.
[28] B. Venkatesh, R. Ranjan, and H. B. Gooi, "Optimal reconfiguration of radial distribution systems to maximize loadability" Power Systems, IEEE Transactions on, 19, 2004, 260-266.
[29] M. Aman, G. Jasmon, A. Bakar, and H. Mokhlis, "Optimum network reconfiguration based on maximization of system loadability using continuation power flow theorem" International Journal of Electrical Power & Energy Systems, 54, 2014, 123-133.
[30] S. H. Li and H. D. Chiang, "Nonlinear predictors and hybrid corrector for fast continuation power flow" Generation, Transmission & Distribution, IET, 2, 2008, 341-354.